REPRINT

PROCEEDINGS OF THE
FOURTH INTERNATIONAL CONFERENCE
ON
NUMERICAL METHODS IN GEOMECHANICS

Volume III

EDMONTON, ALBERTA, CANADA

MAY 31 - JUNE 4, 1982

Crack Band Model for Fracture of Geomaterials

ZDENĚK P. BAŽANT
Professor of Civil Engineering and Director, Center for Concrete and Geomaterials, Technological Institute, Northwestern University, Evanston, Illinois 60201, U.S.A.

SYNOPSIS Due to their heterogeneity, fracture in rocks as well as the artificial rock - concrete - propagates with a dispersed band of microcracks at the front. The progressive formation of the microcracks is described by a triaxial stress-strain relation which exhibits a gradual strain-softening. The stiffness matrix of a material intersected by a system of parallel continuously distributed cracks is obtained in the limit. The area under the stress-strain curve, multiplied by the width of the crack band (fracture process zone) represents the fracture energy. The resulting fracture theory is characterized by three independent parameters, the fracture energy, the tensile strength, and the width of the crack band, the latter being empirically found to approximately equal five-times the grain size in rock. The formulation lends itself easily to a finite element analysis, which is employed to calibrate the theory by fitting various test data on rock fracture available in the literature. Excellent agreement is achieved both with the maximum load data and the R-curve data. A linear fracture theory, which is obtained as the limit for very large sizes of the structure and the finite elements, and the effect of the choice of element size are discussed. Moreover, similarity between the fracture of rocks and of concretes is emphasized and the results obtained in a parallel investigation of concrete are summarized. Finally, fracture analysis from the view point of strain-localization instability is given.

INTRODUCTION

Due to their heterogeneous microstructure and the relatively low strength of interface bonds, many geomaterials, including most rocks as well as the artifical rocks — concretes, exhibit fracture behavior which markedly differs from that of metals, glass, polymers and other materials. In materials for which fracture mechanics was developed first, the crack tip is surrounded by a nonlinear zone which is rather small, and linear fracture mechanics is then applicable. Later nonlinear ductile fracture mechanics was developed for certain metals and other materials in which the nonlinear zone surrounding the crack tip is large compared to the dimension of the specimen (Fig. 1a). An often unpronounced yet important characteristic of these theories is that the fracture process zone, defined as the zone in which progressive microcracking or void formation causes a decrease of stress at increasing strain, remains small. The fracture of geomaterials differs chiefly in the fact that not only the nonlinear zone but also the fracture process zone is large compared to the dimensions of the specimen or structure (Fig. 1c) At the same time, compared to the theories for ductile fracture of metals, we detect one simplifying feature, namely that the nonlinear zone is not much larger than the fracture process zone, permitting us to consider, as an approximation, that all material surrounding the fracture process zone is elastic. Due to this fact, there is no need to employ the J-integral in the analysis; indeed, nonlinear behavior is found only inside the fracture process zone, in which the J-integral cannot be contour-independent as a result of strain-softening and the fact that fracture energy is being consumed all over this zone.

From the continuum mechanics viewpoint, analysis of the fracture process zone is complicated by the fact that a strain-softening continuum is unstable and can in fact be supposed to exist only as a continuous approximation too a heterogeneous microstructure within a sufficiently small region. Due to this difficulty, we will avoid attempting to analyse the distribution of stresses and strains within the fracture process zone and will treat this zone only in a global or average sense.

In the finite element context, this means that the width of the fracture process zone (crack band) may be assumed to coincide with the size of the finite element. The situation is depicted in Fig. 2. Behind the fracture process zone, the microcracks localize into a distinct single continuous crack, the crack which is easily visible to unaided eyes. We take the viewpoint that modelling of the coalescence of microcracks into a single crack is not essential, for the fracture process zone must form first and must propagate through the material before the tip of the continuous crack can propagate. By this argument, we reduce, as an approximation, the analysis of all fracture in geomaterials to the analysis of a propagation of a blunt crack band.

The objective of the present lecture is to summarize and review a series of recent works carried out at Northwestern University (Bažant and Cedolin, 1979, 1980, 1981; Bažant and Oh, 1981; Oh, 1982). The principal characteristic of this line of investigation is the modelling of fracture via stress-strain relations. Although, as we just explained, there are sound physical grounds for taking this approach, we must admit that another important motivation is computational convenience.

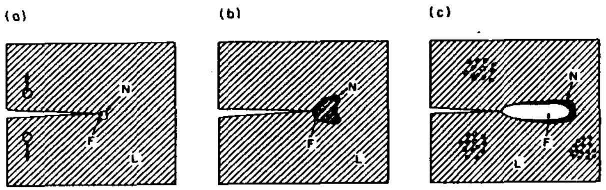

Fig. 1 Illustration of Essential Differences Between (a) Linear Fracture Mechanics, (b) Ductile Fracture Mechanics of Metals With a Large Nonlinear (yielding) Zone, and (c) Rocks and Concretes, (L — Linearly Elastic Zone, N — Nonlinear Hardening Zone, F — Fracture Process Zone Characterized by Strain-Softening).

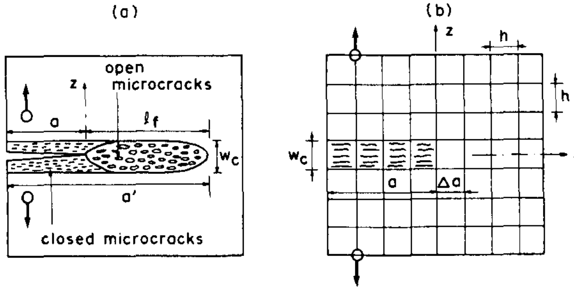

Fig. 2 Fracture Process Zone, Crack Band, Formation of a Sharp Crack, and Finite Element Representation.

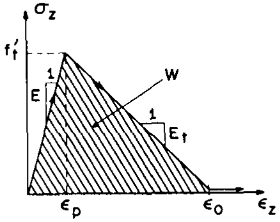

Fig. 3 Uniaxial Stress-Strain Relation Underlying the Present Fracture Model.

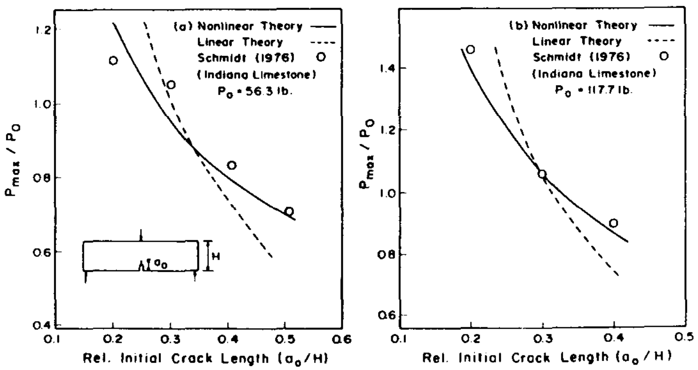

Fig. 4 Fits of the Test Data of Schmidt (1976) for Indiana Limestone.

In the modelling of fracture in finite element analysis, there exist two possibilities: either the cracks are considered to open at the interface of finite elements, or they are modelled as bands of continuously distributed (smeared, dispersed) cracks intersecting the entire finite element. The second approach, introduced in the mid-1960's by Rashid, and Ngo and Scordelis, has prevailed for large finite element codes. While the interelement crack approach requires doubling a node into two nodes as the crack passes through it, and considering the location of the node into which the crack should extend as unknown, in case the correct direction is not given in advance, the smeared crack approach requires only that the element stiffness matrix be redefined after cracking, being replaced by an orthotropic stiffness matrix with a zero stiffness in the direction normal to the cracks. The crack direction is simply characterized by the direction of the axis of material orthotropy. Such a crack band can propagate through a element mesh in an arbitrary direction if we accept the approximation of a smooth curved crack band by a zig-zag band. In the present lecture, we outline an extension of this, by now classical, approach to the modelling of nonlinear fracture, placing emphasis on the applications to rocks.

FULLY CRACKED MATERIAL

Throughout this lecture, we employ cartesian coordinates $x_1 = x_2 = y$, and $x_3 = z$, the cracks being assumed to be normal to the axis z. The normal stress and strain components may be grouped into the column matrices

$$\underset{\sim}{\sigma} = (\sigma_x, \sigma_y, \sigma_z)^T \quad , \quad \underset{\sim}{\varepsilon} = (\varepsilon_x, \varepsilon_y, \varepsilon_z)^T \tag{1}$$

where T denotes the transpose. The strains are assumed to be linearized, or small. The elastic stress-strain relation for the normal components may then be written as

$$\underset{\sim}{\sigma} = \underset{\sim}{D}\,\underset{\sim}{\varepsilon} \tag{2}$$

in which

$$\underset{\sim}{D} = \begin{bmatrix} D_{11} & D_{12} & D_{13} \\ & D_{22} & D_{23} \\ \text{sym.} & & D_{33} \end{bmatrix} \tag{3}$$

$\underset{\sim}{D}$ is the stiffness matrix of the uncracked material.

If the elastic material becomes intersected by continuously distributed cracks normal to z, the stress-strain relation is known (e.g., Suidan and Schnobrich, 1973) to take the form

$$\underset{\sim}{\sigma} = \underset{\sim}{D}^{fr}\,\underset{\sim}{\varepsilon} \tag{4}$$

$$\underset{\sim}{D}^{fr} = \begin{bmatrix} D_{11} - D_{13}^2 D_{33}^{-1}, & D_{12} - D_{13} D_{23} D_{33}^{-1}, & 0 \\ & D_{22} - D_{23}^2 D_{33}^{-1} & , \ 0 \\ \text{sym.} & & 0 \end{bmatrix} \tag{5}$$

This matrix, representing the stiffness matrix of a fully cracked material, is derived from the condition that the stress normal to the cracks must be 0, assuming the material between the cracks to behave as an uncracked elastic material (this is actually a simplification, because often even the material between the cracks may be damaged by presence of discontinuous microcracks).

PROGRESSIVE MICROCRACKING

To describe progressive development of microcracks in the fracture process zone, we need to formulate a stiffness matrix which continuously changes from the form given in Eq. 3 to that in Eq. 5. This objective is not very easy to achieve by direct reasoning, since every element of the 6 x 6 stiffness matrix changes. It was found (Bažant, Oh, 1981), that the task is much easier for the compliance matrix $\underset{\sim}{C}$, in which case

$$\underset{\sim}{\varepsilon} = \underset{\sim}{C}\,\underset{\sim}{\sigma} \tag{6}$$

where

$$\underset{\sim}{C} = \underset{\sim}{D}^{-1} = \begin{bmatrix} C_{11} & C_{12} & C_{13} \\ & C_{22} & C_{23} \\ \text{sym.} & & C_{33} \end{bmatrix} \tag{7}$$

It appears that one needs to consider only one element of the compliance matrix to change:

$$\underset{\sim}{C}(\mu) = \begin{bmatrix} C_{11} & C_{12} & C_{13} \\ & C_{22} & C_{23} \\ \text{sym.} & & C_{33}\mu^{-1} \end{bmatrix} \tag{8}$$

since the following statement (theorem) has been proven (Bažant, Oh, 1981):

$$\underset{\sim}{D}^{fr} = \lim_{\mu \to 0} \underset{\sim}{C}^{-1}(\mu) \tag{9}$$

i.e., the foregoing stiffness matrix of a fully cracked material (Eq. 5) represents the limit of the inverse of the compliance matrix with parameter μ in Eq. 8 as this parameter tends to 0. With regard to numerical programing, it should be noted that instead of setting $\mu = 0$ one assigns in the program μ = a very small number (e.g., 10^{-40}) so as to allow the computer to carry out the inversion of the matrix numerically; the result is a stiffness matrix like that in Eq. 5 except that extremely small numbers (10^{-40}) are obtained instead of 0. For the programmer, this is actually an easier way to write the program than directly setting up Eq. 5.

Comparing now the compliance matrices in Eqs. 7 and 8, we see that a continuous transition from a crack-free state to a fully cracked state may be very simply obtained by a continuous variation of parameter μ, which we call the cracking parameter. The limiting cases are

$$\begin{aligned} &\text{uncracked:} && \mu = 1 \\ &\text{fully cracked:} && \mu = 0 \end{aligned} \tag{10}$$

The variation of the cracking parameter, μ, may be calibrated on the basis of a uniaxial tensile test. From tests carried out in extremely stiff machines or with a stabilization by parallel stiff bars (e.g., Evans and Marathe, 1968), and employing sufficiently small test specimens, it is known that the tnesile stress-strain relation exhibits a gradual decrease of stress at increasing strain, called strain-softening, the softening branch being normally a few times longer than the rising branch. Although this stress-strain relation appears to be smoothly curved, it may be approximated by a bilinear stress-strain relation (Fig. 3). The declining (strain-softening) branch is characterized by compliance C_{33}^t. For uniaxial tension σ_z we can then write

$$\varepsilon_z = C_{33}\mu^{-1}\sigma_z \quad \text{or} \quad \sigma_z = C_{33}^{-1}\mu\varepsilon_z \tag{11}$$

which must be equivalent to the following equation for the straight line of the strain-softening branch:

$$\sigma_z = (\varepsilon_z - \varepsilon_0) / C_{33}^t \tag{12}$$

in which C_{33}^t is negative and ε_0 represents the terminal point of the strain-softening branch at which the tensile stress vanishes (Fig. 3) This point is related to the strain ε_p at the peak stress point as follows

$$\varepsilon_0 = \varepsilon_p + (-C_{33}^t)\, f_t' \tag{13}$$

Comparing Eqs. 11 and 12, we obtain

$$\mu^{-1} = \frac{-C_{33}^t}{C_{33}} \; \frac{\varepsilon_z}{\varepsilon_0 - \varepsilon_z} \tag{14}$$

as the law governing the variation of cracking parameter μ, in correspondence to our assumption of a straight-line strain-softening branch. Substituting Eq. 14 into Eq. 8 and inverting the matrix, we obtain the stiffness matrix $\underset{\sim}{D}$ to be used in the finite element program.

Our use of a straight line for the strain-softening branch is not only simple but also permits us to circumvent the problem of instability which leads to fracture. The formation of the fracture process zone may be regarded as a problem of strain-localization instability of a continuum. This instability depends on the tangent modulus, and if the tension modulus varies continuously, as is the case for a smoothly curved tensile stress-strain relation, the instability which leads to fracture can happen at various points on the strain-softening branch. As a consequence, the work consumed by fracture does not necessarily correspond to the complete area under the stress-strain curve, since it is governed by the unloading slope from the point of instability. Due to our choice of a straight-line strain-softening branch, the tangent modulus is constant on the entire branch, and so if the fracture should occur, it must occur right at the peak stress point, in which case the work consumed by fracture corresponds to the complete area under the stress-strain curve. This fact considerably simplifies further analysis.

Many rocks may be considered isotropic, and normally this is also a very good assumption for concrete. The compliance and stiffness matrices for partially cracked concrete then take on the following special forms

$$\underset{\sim}{C}(\mu) = \frac{1}{E}\begin{bmatrix} 1 & -\nu & -\nu \\ -\nu & 1 & -\nu \\ -\nu & -\nu & \mu^{-1} \end{bmatrix} \tag{15}$$

and for $\mu \to 0$:

$$\underset{\sim}{D}^{fr} = \frac{E}{1-\nu^2}\begin{bmatrix} 1 & \nu & 0 \\ \nu & 1 & 0 \\ 0 & 0 & 0 \end{bmatrix} \tag{16}$$

in which E = Young's modulus and ν = Poisson's ratio.

In computer finite element analysis, it is most convenient to use the incremental loading technique. For this purpose, the incremental stress-strain relations are obtained by differentiating Eq. 6 in which the compliance matrix from Eq. 7 with μ from Eq. 14 is substituted. In a finite element program, it is also necessary to enlarge the compliance and stiffness matrices to a 6x6 form, including the rows and columns for shear strains and stresses. Most simply, these may be considered the same as for a crack-free material, except that the shear stiffness in the diagonal term is reduced by an empirical shear stiffness reduction factor (Suidan, Schnobrich, 1973). More accurately, the columns and rows for the shear behavior should reflect the frictional-dilatant properties of cracks (see, e.g., Bažant, Gambarova, 1980; Bažant, Tsubaki, 1980). The question of shear terms is, however, usually unimportant since the fracture in geomaterials takes place in principal stress planes and leads to principal strains which are parallel. The only case, where the shear terms matter is when the direction of principal stresses continuously rotates during the progressive microcracking. We will comment on this case later.

Absence of a significant rotation of the principal stress direction during the passage of the fracture process zone through a fixed station justifies another simplifying assumption which is implied in our preceding formulation. It is a fact that the total stress-strain relations which are employed (Eqs. 6, 8) are path-independent. In reality, all inelastic behavior is of course path- dependent. Nevertheless, the assumption of path-independence of the stress-strain relation in the vicinity of the crack front has already been proven to be acceptable in other nonlinear fracture problems, particularly in the theory of ductile fracture, in which the application of Rice's J-integral is contingent upon the validity of this assumption.

A characteristic feature of the compliance matrix for progressive microcracking (Eq. 7) is the absence of Poisson effect with regard to the cracking. This feature may be justified on physical grounds if we assume all microcracks to be normal to axis z. This is certainly a simplifying assumption, and in reality we must assume a certain distribution of the orientations of the microcracks, the orientation normal to axis z being the prevalent one. If inclined microcracks were considered, then it would be necessary to also change the off-diagonal terms in Eq. 7 as the formation of microcracks advances.

The difference of the actual strain ε_z at the strain-softening branch from the strain predicted for an uncracked material (Bažant, Oh, 1981) represents the average strain, ε_f over the width of the fracture process zone caused by microcracking. If this strain is integrated over the width of the crack band, one may obtain from our stress-strain relation a stress-displacement relation. For the models in which the fracture is treated as a sharp interelement crack, this displacement is analogous to the opening displacement of such a crack. In this regard we should note that softening stress-displacement relations were used to model nonlinear fracture in many preceding works, which provided

inspiration for our model (Barenblatt, 1959; Kfouri, Miller, 1974, Wnuk, 1974; Knauss, 1974; Kfouri, Rice, 1977; Hillerborg, Modéer, Petersson, 1976; Petersson, 1980). Among these works, the pioneering original contribution* by Hillerborg et al. (1976) was concerned with concrete. All these works were however characterized by the use of a sharp crack (fictitious crack), which seems computationally not as convenient as the smeared crack band approach, and may be unrealistic in the cases in which the finite width of the fracture process zone which propagates ahead of the sharp crack is of importance.

Although we cannot treat it in detail, it is interesting to observe that the smeared crack band approach lends itself logically to describing the effect on fracture of the triaxial stress state in the vicinity of the crack front. From extensive testing, it is known that in the presence of transverse normal compression stresses, the tensile strength is diminished. The measured biaxial failure envelopes seem to consist approximately of straight lines connecting the failure points for uniaxial tensile failure and for uniaxial compression failure in the (σ_x, σ_y) plane. Accordingly, we may suppose that transverse compressive stresses reduce the peak stress (Fig. 3) by

$$\Delta f_t' = k(\sigma_x + \sigma_y)\ , \qquad k = f_t' \,/\, f_c' \tag{17}$$

where f_t' = uniaxial tensile strength and f_c' = uniaxial compression strength. Thus we have

$$\begin{aligned} &\text{for} \quad \Delta f_t' \le 0 : f_{tc}' = f_t' + \Delta f_t' \\ &\text{for} \quad \Delta f_t' > 0 : f_{tc}' = f_t' \end{aligned} \tag{18}$$

It is worth noting that our treatment of progressive microcracking by reducing material stiffness with a multiplicative parameter (as in Eq. 8) bears some similarity with the so-called continuous damage mechanics, which has recently been applied to concrete by Løland (1980), Lorrain (1981), Mazars (1981) and others. Our approach is however fundamentally different in that our treatment of damage is tensorial rather than scalar, and that the damage due to microcracking is considered to be inseparable from a zone of a certain characteristic width, w_c.

MATERIAL FRACTURE PARAMETERS

The fracture energy defined as the energy consumed by crack formations per unit area of the crack plane, may be calculated as

$$G_f = W_f\, w_c \tag{19}$$

in which w_c = width of the crack band (fracture process zone) and W_f = work of tensile stress = area under the tensile stress-strain curve (Fig. 3), i.e.,

$$W_f = \int_0^{\varepsilon_0} \sigma_z\, d\varepsilon_z \tag{20}$$

*Hillerborg et al, (1976) were first to formulate a fictitious crack model for concrete which, in contrast to our model, is based on a softening relation between stresses and displacement in the extension of a sharp crack.

In theory, it should be possible to determine the crack band width w_c by analyzing the strain-localization instability that leads to fracture. It should be possible to do this by extending the previous simple analysis of this instability by Bažant (1976) and Bažant and Panula (1978). This would however be quite complicated in case of a large fracture process zone within a nonhomogeneously stressed specimen. Aside from that, since w_c ought to be a material property, it can be determined empirically and can be considered as a constant. This is necessary to make the calculation results independent of the choice of the finite element size, as has been demonstrated numerically (Bažant, Oh, 1981).

For the bilinear tensile stress-strain relation (Fig. 3), we have

$$W_f = \frac{1}{2}\,(C_{33} - C_{33}^t)\, f_t'^2\, w_c = \frac{1}{2}\, f_t'\, \varepsilon_0 \tag{21}$$

From this relation we may calculate

$$w_c = \frac{2G_f}{f_t'^2}\; \frac{1}{C_{33} - C_{33}^t} \tag{22}$$

in which C_{33}^t is negative. This equation indicates that the width of the fracture process zone, precisely the effective width corresponding to a uniform transverse distribution of tensile strain over the crack band, may be determined by measuring the softening compliance, the tensile strength, and the fracture energy.

In relation to fracture models utilizing stress-displacement relations for sharp cracks, it seems that the precise width w_c of the fracture process zone should not be very important, provided that correct energy dissipation by the crack formation is assured. In other words, we should get essentially the same results utilizing different widths of the crack band, provided we adjust the softening compliance C_{33}^t so as to assure that the energy consumed in the fracture process zone equals the given value G_f. Thus, we may choose the value w_c, and then we may calculate C_{33}^t from Eq. 22, thereby assuring the energy consumption to be correct. It has been numerically demonstrated (Bažant, Oh, 1981) that indeed the analyses with different w_c yield essentially the same numerical results. If we however insist on using the correct experimentally observed softening compliance C_{33}^t, then the actual value of the crack band width w_c must be used (and in this manner then Eq. 25 given later was determined).

To assure that C_{33}^t be negative (or else the stress-strain relation would not terminate with a fully cracked state), Eq. 21 indicates that the following condition must be met

$$w_c < w_0, \quad w_0 = \frac{2G_f E}{f_t'^2} \tag{23}$$

The case when the slope of the strain-softening branch is very small is also inadmissible for practical purposes. Therefore, the size of the finite element should be distinctly less than the values w_0 given by Eq. 23. Since typically $C_{33}^t = -C_{33}$, it appears suitable to use finite elements of width

$$h \simeq w_0/4 \qquad (24)$$

VERIFICATION BY TEST DATA

The foregoing mathematical model, which was first developed and applied with a great deal of success to concrete (Bažant, Oh, 1981), has been fitted by Oh (1982) too various test data on rock fracture tests available in the literature. The optimum fits achieved are shown by the solid lines in Figs. 4-10. For comparison, the best possible fits according to the classical linear fracture theory are also shown in these figures, as the dashed lines. The material parameters corresponding to the fits shown are summarized in Table 1. All fits were calculated by the finite element method, using rectangular finite elements each of which consists of four constant strain triangles. A plane stress state was assumed for all calculations. The stress-strain relation we just developed was assumed to hold for all finite elements but using small enough loading steps the softening state was reached only within one row of finite elements. The tangent stiffness was assumed to be the same for all four triangles composing a rectangular element and was determined from the average of the strains in the four triangles.

In a preceding analysis (Bažant, Oh, 1981) of twenty-two test series on the fracture of concrete reported in the literature — quite a large statistical sample indeed — it was discovered that the optimum width of the crack band (fracture process zone) is roughly $w_c \simeq 3d_a$ where d_a represents the maximum size of the aggregate in concrete. It is for this width w_c that the area under the stress-strain curve yields the correct value of the fracture energy needed to obtain good fits of the test data. Having this finding in mind, the fits of all fracture test data presented here were sought under the restriction that the ratio w_c/d_g where d_g = grain size, be the same for all test data for the various rocks considered, and only the values of G_f and f_t' were considered to vary from rock to rock (Table 1). This analysis led to the following rather useful result:

$$w_c \simeq 5d_g \qquad (25)$$

Due to this relation, as well as the previously derived energy relation (Eq. 21), our nonlinear fracture theory is a two-parameter theory, the two material parameters to be determined by experiment being G_f and f_t'. We should however consider Eq. 25 as tentative since it rests mainly on the experimental results of Hoagland et al. (1973); the statistical sample available for rock in the literature is much smaller than that available for concrete.

Test data in Figs. 4-7 (Schmidt, 1976; Carpinteri, 1980; Schmidt, Lutz, 1979), obtained for Indiana limestone, Carrara marble, Colorado oil shale, and Westerly granite, give the maximum loads P_{max} achieved in the fracture tests. These values are reported in terms of the ratios P_{max}/P_0 where P_0 is the maximum load which follows by applying the bending theory. In Fig. 4, $P_0 = 2BH^2 f_t'/3L$ = maximum load based on bending theory calculation for an uncracked beam, where H = beam depth, B = beam thickness, L = beam span, and f_t' = tensile strength. The same definition of P_0 was used for Figs. 5 and 6. For the tests in Fig. 7, $P_0 = WBf_t'$ where W = specimen width, and B = its thickness. The maximum loads P_{max} were obtained with the finite element code simply by increasing the displacements at the loading points in small increments, calculating at each loading step the reaction at the loading point, and thus identifying the maximum reaction. The linear theory results, shown by the dashed lines, were calculated according to the blunt crack band approach (Bažant, Cedolin, 1979, 1980), considering a sudden stress drop and a finite element version of the energy release criterion.

Fig. 8 shows the fits of the data by Hoagland et al. (1973) and Schmidt and Lutz (1979) on the R-curves (resistance curves), in which the apparent fracture energy determined from the tests is plotted as a function of the crack extension (in slow stable crack growth). According to the classical linear fracture mechanics, this apparent fracture energy would be a constant, and so the dashed line is horizontal and is made to pass through the terminal measured values at which the apparent fracture energy value stabilizes.

To evaluate the errors, we may construct the plot of $Y = P_m/P_0$ vs. $X = P_t/P_0$, in which P_m = measured P_{max}, P_t = theoretical P_{max}, and P_0 = failure load based on strength as defined before. All the data points from Figs. 4-7, the number of which totals M = 35, are plotted in this manner in one figure (Fig. 9). Furthermore, in Fig. 10, the same plot is shown for the results of linear theory. Since the ratio X generally decreases with the size of the specimen, the points at the top right of this plot pertain to small specimens and those at left bottom to large specimens.

If our theory were perfect, then the plot of Y vs. X would have to be a straight line having slope 1.0 and passing through the origin. The regression line of this plot, $Y' = a+bX$, must have a close to 0 and b close to 1.0 if the optimum fits have been correctly determined. The errors, i.e., the vertical deviations of data points Y_i from the regression line, may be characterized by the coefficient of variation, ω,

$$\omega = \frac{s}{\bar{Y}}, \quad s^2 = \frac{1}{n-2}\sum_{i=1}^{n}(Y_i - Y')^2, \quad \bar{Y} = \frac{1}{n}\sum_{i=1}^{n} Y_i \qquad (26)$$

where n = number of data points in the plot, and s = standard error. From Fig. 9 we calculate:

For our fracture theory (Fig. 9):	$\omega = 0.106$	
For linear fracture theory (Fig. 10):	$\omega = 0.452$	(27)
For the strength criterion:	$\omega = 0.796$	

The last value for the strength criterion is simply a statistics of the population of P_m/P_0 - values. As another statistical characteristic, one may calculate the coefficient of variation of the population of the values of $X = P_m/P_t$; these are

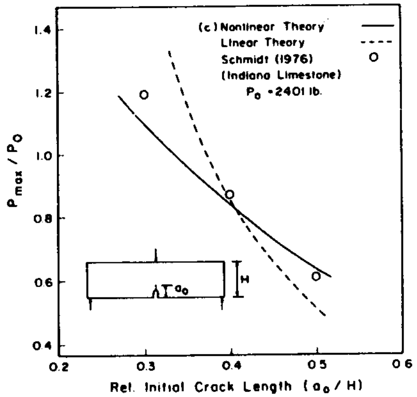

Fig. 4 Continuation

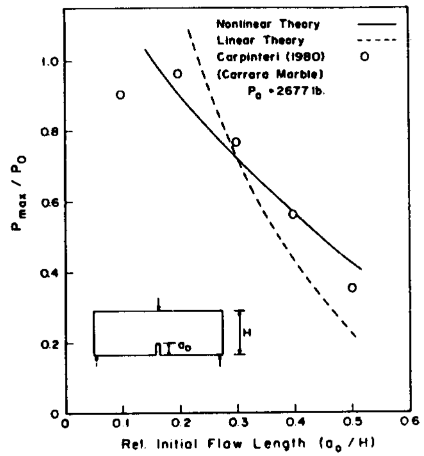

Fig. 5 Fit of the Maximum Load Data of Carpinteri (1980) For Carrara Marble.

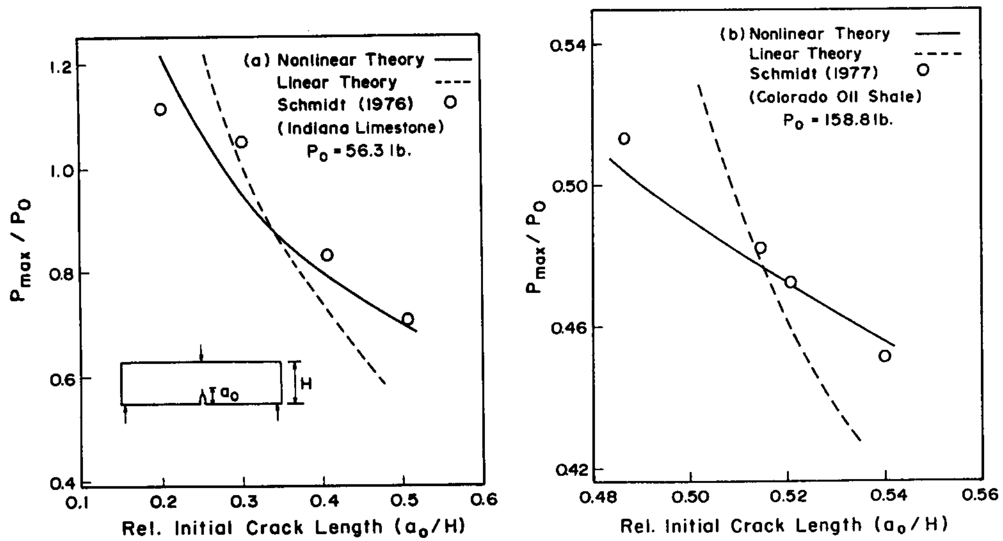

Fig. 6 Fit of the Maximum Load Data of Schmidt for Colorado Oil Shale and Indiana Limestone.

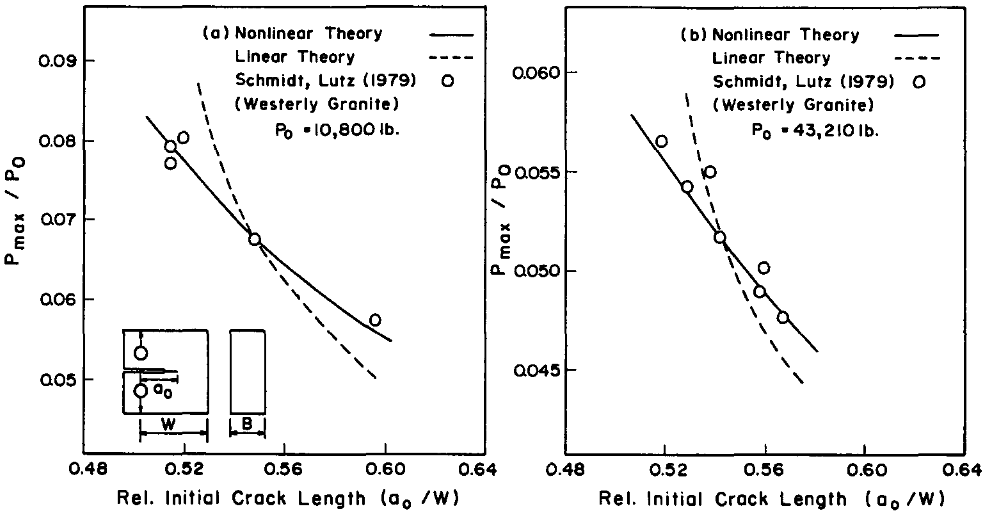

Fig. 7 Fits of the Maximum Load Data of Schmidt and Lutz (1979) for Westerly Granite.

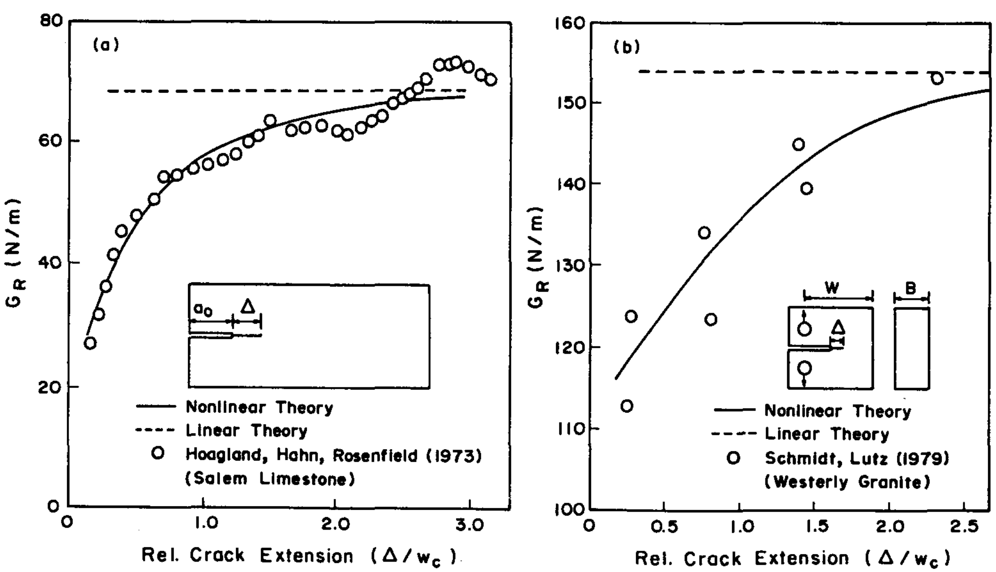

Fig. 8 Apparent Fracture Energy vs. Crack Extension According to Hoagland et al. (1973) for Salem Limestone and Schmidt and Lutz (1979) for Westerly Granite.

$$\begin{array}{ll} \text{For our fracture theory:} & \omega = 0.069 \\ \text{For linear fracture theory:} & \omega = 0.393 \end{array} \tag{28}$$

For a statistical analysis of the errors in the R-curve, it is appropriate to normalize the fracture energy with regard to the internal force transmitted by the fracture process zone, which is roughly proportional to $f'_t d_g$, d_g being the grain size. Accordingly, we may plot the values of $\ell n\ (G_f/f'_t d_g)$ taken from Fig. 8. On the Y-axis we use the measured value G_m of G_f, and on the X-axis we use the theoretical value G_t of G_f. Again, if the theory were perfect, this plot would have to be a straight line $Y = a+bX$ with $a = 0$ and $b = 1$, and thus a linear regression may be carried out. The standard error for the vertical deviation from the regression line may then be calculated to be

$$\begin{array}{ll} \text{For our fracture theory:} & s = 0.046 \\ \text{For linear theory:} & s = 0.222 \end{array} \tag{29}$$

Figs. 9-10 also show as dashed lines the 95% confident limits corresponding to ω or s. These curves are hyperbolas but due to the large size of our statistical samples they are almost straight passing at a vertical distance $\pm$ 1.96 ω or $\pm$ 1.96 s from the regression line.

From this statistical analysis we conclude that our nonlinear theory is capable of satisfactorily describing the available experimental evidence on the fracture of rock (Oh, 1982).

LINEAR THEORY FOR LARGE BODIES AND STRUCTURES

In Eq. 23, we gave an upper limit for the finite element size to be used for our nonlinear fracture theory. This does not mean however that one cannot use larger finite elements. The finite elements can be much larger than the value in Eq. 23, but then one must consider a sudden stress drop. In this case, which is the case of bodies or structures far larger than the grain size, the criterion of crack band extension is simply the energy criterion, which was developed previously (Bažant, Cedolin, 1979; Bažant 1980). Instead of actually implementing this energy criterion in the finite element program, one may approximately achieve the correct energy dissipation due to fracture by adjusting the value of the tensile strength, i.e., using the so-called equivalent strength. According to Eq. 23, its value should be

$$(f'_t)_{eq} = \sqrt{\frac{2EG_f}{w_c}} \tag{30}$$

After σ_z (maximum principle stress) reaches this limit, one must consider σ_z to drop abruptly to 0 (Fig. 11).

As the size of the structure, and thus the size of the finite element, increases to very large values, the value of the equivalent strength (Eq. 28) obviously tends to 0. In the limit we thus obtain the no-tension material, pioneered in mid 1960's by Zienkiewicz, as the correct approach to the fracture mechanics of large rock masses fractured in Mode I. This is of course applicable only in those cases where the use of large finite elements is acceptable.

It may be noted, and this has been a frequent experience for various concrete structures, that often the magnitude of the tensile strength has little effect on the prediction of failure loads of various structures. This is the case of fracture-insensitive problems. In such situations, one of course does not need to bother with applying fracture mechanics or nonlinear fracture mechanics. To determine whether this is the case, the analyst should carry out his calculations twice — once for the actual strength value and once for zero strength value, and if the results of both calculations are essentially the same, then fracture mechanics need not be used.

It is important to realize that the method of blunt crack band coupled with an energy criterion for an abrupt stress drop at fracture gives results which are in excellent

TABLE 1. Parameters for Test Data

Test Series	f'_t (psi)	E (ksi)	G_f (lb./in.)	d_g (in.)	w_c (in.)	$G_f^{\ell in}$ (lb./in.)
1. Schmidt(1976) No. 1	356*	3,130*	0.068*	0.0787+	0.3935	0.027*
2. 2	356*	3,130*	0.068*	0.0787+	0.3935	0.186*
3. 3	356*	3,130*	0.068*	0.0787+	0.3935	1.751*
4. Schmidt(1979) No. 1	768*	3,600*	0.121*	0.0197+	0.0985	0.162*
5. 2	477*	2,232*	0.076*	0.0197+	0.0985	0.168*
6. Carpinteri	725*	2,200*	0.392*	0.0079+	0.0395	0.530*
7. Schmidt, Lutz No. 1	1394*	3,300*	0.874*	0.0296	0.1480	1.697*
8. 2	1394*	3,300*	0.874*	0.0296	0.1480	0.806*
9. 3	1394*	3,300*	0.874*	0.0296	0.1480	0.879*
10. Hoagland, Hahn, Rosenfield	427*	2,000*	0.374*	0.0787	0.3940	0.390*

Note: psi = 6895 N/m^2, lb./in. = 175.1 N/n, in. = 25.4mm, ksi = 1000 psi.

*asterisk indicates numbers estimated by calculations; without asterisk - as reported.

+plus indicates numbers provided by authors or other references.

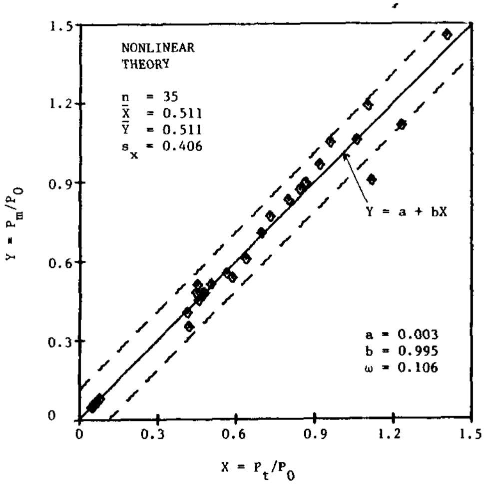

Fig. 9 Statistical Regression Analysis of Maximum Load Data from Figs. 4-7 According to Present Nonlinear Theory

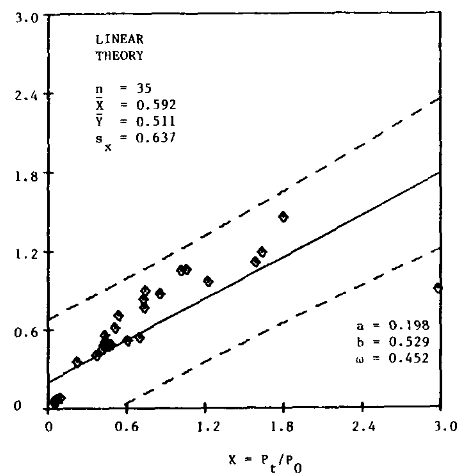

Fig. 10 Same as Fig. 9 but for Optimum Fits by Linear Theory (for comparison)

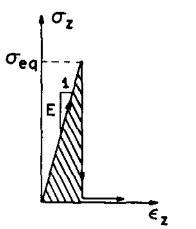

Fig. 11 Abrupt Stress Drop to Be Used When the Element Is Very Large

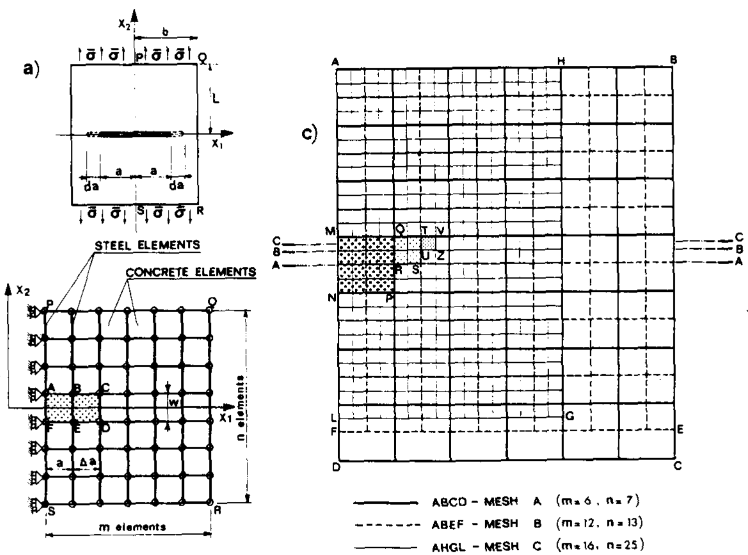

Fig. 12 (a-c) Example of a Center-Cracked Rectangular Panel and Finite Element Meshes Used (after Bažant, Cedolin, 1980).

agreement with the exact solutions for sharp cracks and approximate these solutions just as well as the inter-element crack approach. This has been demonstrated by Bažant and Cedolin (1979) and one of these demonstrations is shown in Fig. 13 in which the load parameter is plotted versus the crack length. The specimen in this calculation was a rectangular panel with a center crack, loaded by a uniform stress at top and bottom. The calculation has been carried out for three different meshes shown in Fig. 12, with finite element sizes in the ratios 4:2:1. The exact solutions are slightly different for each case because the size of the specimen for the three meshes was not exactly the same.

The method which is currently used in all large finite element codes is to determine propagation of distributed (smeared) cracking from one element to another on the basis of the tensile strength criterion. It has been known for a long time that such a calculation cannot converge to correct results, since refinement of the element size to 0 leads to infinite stress concentrations just ahead of the front cracked element, so that the load needed for further extension of the crack tends always to 0. It has not been however generally recognized that the use of the strength criterion can lead to very large errors. As demonstrated by Bažant and Cedolin (1980), the differences in the results can be as large as 100% when the finite element sizes differ as 4:2:1. This is demonstrated by the numerical finite element results in Fig. 13, where the failure load needed for further extension of the crack band is plotted for the same panel as in Fig. 12 against the length of the crack band. The curves obtained for meshes A, B, C of finite element sizes 4:2:1, are seen to be very far apart, whereas the curves for the finite element results obtained with the energy criterion for the abrupt stress drop agree with each other, the difference being negligible and tending to 0 as the mesh is refined.

CRACKS IN SKEW DIRECTION IN THE MESH

In a general situation the crack direction would not be parallel to the mesh line, as in our foregoing analysis of test specimens. A smoothly curved crack or crack band is then conveniently represented as a zig-zag crack band in the finite element mesh; see Fig. 14. Referring to the notation defined in this figure, the effective width of the crack band to be used in the fracture theory is, for a square mesh of step h,

$$w_c = \frac{h}{\cos\alpha} \tag{31}$$

where α = angle of the crack direction with the mesh line. This condition simply follows from the requirement of an equal area of the zig-zag crack band and a smooth crack band in the direction of the cracks.

TENSORIAL GENERALIZATION AND CURVED SOFTENING

In presence of tensile principal stresses in more than one direction, the preceding stress-strain relation (Eq.6,8) may be generalized as follows

$$\begin{Bmatrix} \epsilon_x \\ \epsilon_y \\ \epsilon_z \end{Bmatrix} = \begin{bmatrix} \mu_x^{-1} C_{11} & C_{12} & C_{13} \\ & \mu_y^{-1} C_{22} & C_{23} \\ \text{sym.} & & \mu_z^{-1} C_{33} \end{bmatrix} \begin{Bmatrix} \sigma_x \\ \sigma_y \\ \sigma_z \end{Bmatrix} \tag{32}$$

Here μ_x, μ_y, μ_z are cracking parameters for x, y, z directions, analogous to parameter μ used before. For the same reasons as before, we consider that gradual cracking requires modifying only the diagonal coefficients of the compliance matrix in Eq. 32. Parameters μ_x, μ_y, and μ_z are in general functions of the strain tensor ϵ_{ij} (or σ_{ij}).

To model real fracture processes more accurately, we should consider that the softening stress-strain diagram can be generally and smoothly curved. Furthermore, in real situations it may frequently occur that the directions of the principal stresses rotate during the progressive microcracking that leads to fracture. For this purpose, we need to generalize Eq. 32 into a tensorial form, guaranteeing fulfillment of tensorial invariance conditions. This may be accomplished by the following secant tensorial stress-strain relation

$$\epsilon_{ij} = C^{sec}_{ijkm}\,\sigma_{km} \tag{33}$$

in which

$$C^{sec}_{ijkm} = C^{e\ell}_{ijkm} + b\,\epsilon_{ik}\,\epsilon_{jm} \tag{34}$$

in which subscripts i, j, k, m refer to cartesian coordinates x_i (i = 1,2,3), C^{sec}_{ijkm} is the tensor of secant compliances and $C^{e\ell}_{ijkm}$ is the tensor of elastic compliances, expressed for an isotropic material in terms of E, ν; and b is a scalar parameter. It may be checked that the term $\epsilon_{ik}\,\epsilon_{jm}$ modifies only the diagonal coefficients in the compliance matrix and that Eq. 34 reduces to Eq. 22 when the principal stress and strain directions coincide and principle coordinates are used. In particular, Eqs. 33-34 yield the following expressions for the cracking parameters

$$\mu_x^{-1} = 1 + Eb\epsilon_x^2,\quad \mu_y^{-1} = 1+Eb\epsilon_y^2,\quad \mu_z^{-1} = 1+Eb\epsilon_z^2 \tag{35}$$

Parameter b may in general be a scalar function of stresses and strains, and by comparison with the typical shapes of the tensile softening curve a suitable form appears to be

$$b = \beta e^{c\,\epsilon_{kk}} \tag{36}$$

in which case Eq. 32, when written for uniaxial tension, reduces to the form

$$\sigma_z = \frac{E\epsilon_z}{1 + \beta\,\epsilon_z^2\, e^{c\epsilon_{kk}}},\quad \epsilon_x = \epsilon_y = -\frac{\nu}{E}\sigma_z \tag{37}$$

where β = constant (depending on the strength of concrete). We should also note that due to the use of an exponential in Eqs. 36-37, the stress-strain diagram in compression is different from that in tension, and for sufficiently large exponent coefficient c (a constant) the occurrence of strain-softening in compression may be suppressed

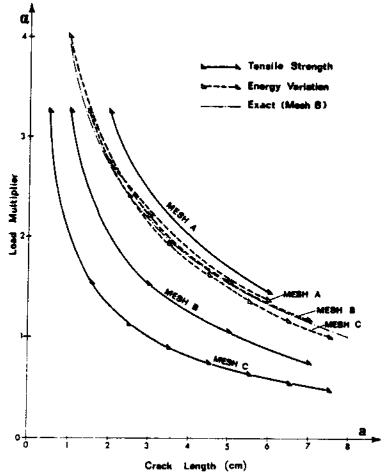

Fig. 13 Numerical Results for the Example in Fig. 12 and Exact Solution for a Sharp Crack (after Bažant, Cedolin, 1980).

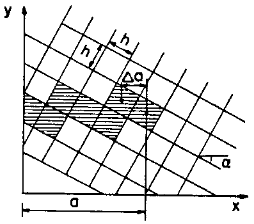

Fig. 14 Representation of Skew Fracture Propagation by a Zig-Zag Crack Band

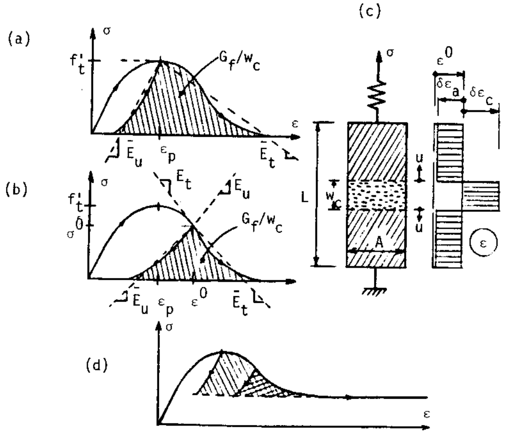

Fig. 15 Energy Release Due to Strain-Localization Instability and Tensile Specimen Serving as a Model to Fracture Process Zone.

making the compression behavior linear. We should however realize that Eq. 34 still cannot describe the complete behavior in compression; in particular, Eq. 34 does not reflect the plastic component of deformations under high isostatic compression and the microfracturing under high compression stresses parallel to the microcracks.

Is it possible that there exist other tensorial generalizations than that in Eqs. 33-34? If we restrict attention to quadratic terms in strain in Eq. 34, it is not. One may check this by trying all possible permutations of subscripts in the term $\epsilon_{ik}\epsilon_{jm}$. We should especially observe that the terms of the type $\epsilon_{ij}\epsilon_{km}$ are inadmissible since they do not reduce to Eq. 32. On the other hand, the use of loading surfaces, $\Phi(\epsilon) = 0$, always leads to terms of the type $\partial\Phi/\partial\epsilon_{ij}$ and $\partial\Phi/\partial\epsilon_{km}$, which always produces terms of the form $\epsilon_{ij}\epsilon_{km}$ rather than $\epsilon_{ik}\epsilon_{jm}$ when quadratic terms are considered. We thus arrive at an interesting conclusion:

The use of loading surfaces cannot provide a correct compliance matrix for the description of progressive microcracking which leads to complete fracture.

This means, especially, that the plastic-fracturing theory (Bažant, Kim, 1979), formulated to describe microcracking under compressive and shear loadings, cannot be extended to formulate tensile strain-softening up to complete fracture. This theory was based on the use of loading surfaces in the stress and strain spaces.

The picture of the stress-strain diagram given by Eq. 37 is shown in Fig. 15. To describe the fact that compressive stresses σ_x and σ_y in the directions parallel to the crack plane reduce the tensile strength (peak stress), it may be appropriate to further introduce parameter β as a function of the principal stresses in the directions parallel to the crack plane.

STRAIN-LOCALIZATION INSTABILITY

The formation of fracture through a gradual deformation of a finite fracture process zone should properly be discussed as an instability of a nonlinear continuum, in which a uniformly distributed strain localizes into a softening band of finite width, w_c, at the boundary of which there is a jump in the value of strain. With regard to shear failures, the concept of strain-localization instability was analyzed in detail by Rice (1976) and others, with particular attention to the effect of geometric nonlinearities. A stability analysis of strain-localization in tension, with particular attention to finite size bodies and to the effect of differences between the tangent loading modulus and the tangent unloading modulus in the strain-softening regime, was presented by Bažant (1976) and Bažant and Panula (1978). Fundamental to the stability analysis is the sign of the energy change due to strain localization.

Consider the work ΔU which must be supplied externally to the structure to advance the crack band by distance Δa. According to Bažant and Cedolin (1979, 1980) this work may be expressed as

$$\Delta U = G_f\Delta a - \Delta U_0 - \Delta U_1 \qquad (38)$$

in which

$$\Delta U_0 = \int_{\Delta V} \frac{1}{2}\left(\sigma_{ij}^0\,\epsilon_{ij}^0 - \sigma_{ij}\epsilon_{ij}\right) dV \qquad (39)$$

$$\Delta U_1 = \int_{\Delta S} \frac{1}{2}\,\Delta T_i^0\,(u_i - u_i^0)\, dS \qquad (40)$$

Here ΔV is the volume of the element into which the crack band extends during the jump Δa in length, and ΔS is the boundary of this element; ΔU_0 is the strain energy released from volume ΔV due to the formation of microcracks, and ΔU_1 is the energy transferred into volume ΔV (fracture process zone) from the surrounding structure; σ_{ij}^0 and ϵ_{ij}^0 are the initial stresses and strains in ΔV before fracture, and σ_{ij}, ϵ_{ij} are their values after fracture; u_i^0 are the displacements at the boundary ΔS before fracture and u_i are those after fracture; and ΔT_i^0 are the boundary tractions which balance the initial stresses σ_{ij}^0 in the sourrounding structure as the stresses in volume ΔV are reduced from σ_{ij}^0 to σ_{ij}. In case of plane stress and isotropic material, we have

$$\sigma_{ij}\epsilon_{ij} = E'\epsilon_{11}^{0\,2}, \quad E' = E/(1-\nu^2) \qquad (41)$$

If the required work ΔU is positive, then no change can happen if this work is not externally supplied, i.e., the crack band is stable (does not advance). If ΔU is negative, no work needs to be supplied but work is released by the fracture, i.e., fracture can occur spontaneously and the energy release $-\Delta U$ goes into kinetic energy. If $\Delta U = 0$, we have a critical state in which fracture can occur statically, since no excess energy is available to produce kinetic energy. Thus, the stability conditions are

$$\begin{aligned} \Delta U &> 0 \quad \text{stable} \\ \Delta U &= 0 \quad \text{critical (unstable)} \\ \Delta U &< 0 \quad \text{unstable} \end{aligned} \qquad (42)$$

Following previous work (Bažant, 1976), it is quite instructive to analyze in this manner the failure of a uniformly stressed specimen subjected to uniaxial tension (Fig. 15c). We may imagine such a specimen to serve as an approximate model for volume ΔV of the fracture process zone. We assume the specimen to be loaded through a spring of spring constant C which models either the spring constant of a testing machine or the elastic support of the fracture process zone by the surrounding structure. Let the cross section of the specimen be A = 1. The appearance of the crack band in the specimen may be considered as a sudden finite jump by distance $\Delta a = 1$ in which the front of the crack band moves from the left to the right face of the specimen (Fig. 15c). For a uniaxial stress state in the specimen (of length L), Eqs. 38 and 39 take the form

$$\Delta U_0 = \frac{w_c}{2}\sigma^0\epsilon^0 = \frac{w_c}{2}\sigma^0\frac{\sigma^0}{E_u} \qquad (43)$$

$$\Delta U_1 = \frac{1}{2}\sigma^0(\Delta u - \Delta u_0) = \frac{1}{2}\sigma^0\left[(L - w_c)\frac{\sigma^0}{E_u} + \frac{\sigma^0}{C}\right] \qquad (44)$$

in which we drop subscripts z from σ and ε, and $\Delta u - \Delta u_0$ is the change in the relative displacement between the opposite faces of the crack band of width w_c, and $\bar{E}_u$ is the average unloading modulus (Fig. 15c).

Alternatively, we can calculate ΔU from the changes of strains ε_c in the crack band and ε_a outside the crack band. To satisfy equilibrium in the tensile specimen in Fig. 15c, the stress change $\delta\sigma$ must be the same inside the crack band and outside the crack band, and thus

$$\delta\varepsilon_c = \delta\sigma/E_t,\ \delta\varepsilon_a = \delta\sigma/E_u \tag{45}$$

The energy consumed in the crack band and the energy released from the rest of the specimen may now be calculated as follows

$$\Delta U_c = \frac{w_c}{2}\ \delta\sigma\delta\varepsilon_c = w_c \frac{(\delta\sigma)^2}{-2E_t} \tag{46}$$

$$\begin{aligned} \Delta U_a &= \frac{1}{2}\,\delta\sigma \left[(L-w_c)\ \delta\varepsilon_a + \frac{\delta\sigma}{C} \right] \\ &= (L-w_c)\frac{(\delta\sigma)^2}{2E_u} + \frac{(\delta\sigma)^2}{2C} \end{aligned} \tag{47}$$

Expressing the stability conditions similarly to Eq.42, we may now write

$$\Delta U = \Delta U_c - \Delta U_a \quad \begin{cases} > 0 & \text{stable} \\ = 0 & \text{critical (unstable)} \\ < 0 & \text{unstable} \end{cases} \tag{48}$$

Considering a finite stress change from σ^0 to 0, i.e., $\delta\sigma = -\sigma^0$, for which we must replace E_u and E_t in Eqs. 46-47 with the average unloading modulus $\bar{E}_u$ and the average tangent modulus $\bar{E}_t$ ($\bar{E}_t < 0$), we may substitute Eqs. 38, 43, 44, 46, and 47 into the equality $\Delta U = \Delta U_c - \Delta U_a$. This furnishes us the following expression for the fracture energy

$$\bar{G}_f = w_c \left(\frac{\sigma^{0^2}}{2\bar{E}_u} + \frac{\sigma^{0^2}}{-2\bar{E}_t} \right) \tag{49}$$

in which we place a bar on top of G_f to indicate that this is an apparent fracture energy value. It is not a constant since it depends on the stress σ^0 at which the fracture begins, which is not necessarily equal to peak stress σ_p.

In case that the instability which produces fracture happens right at the peak stress point, Eq. 49 provides

$$G_f = \frac{w_c}{2} \left(\frac{1}{\bar{E}_u} + \frac{1}{-E_t} \right) \sigma_p^2 \tag{50}$$

which is a constant and represents the fracture energy value corresponding to the value we used in our fracture model to fit this data. The value of G_f is characterized by the cross-hatched area in Fig. 15c limited by the unloading and the softening branches beginning from the peak stress point.

The value of stress σ^0 at which the instability begins may be determined from Eq. 48 by substituting Eqs. 46-47. For the instability which leads to complete failure, i.e., $\delta\sigma = -\sigma^0$ (stress is relieved to 0), we thus obtain the condition

$$\frac{-\bar{E}_t}{\bar{E}_u} = \frac{1}{\dfrac{L}{w_c} - 1 + \dfrac{\bar{E}_u}{Cw_c}} \tag{51}$$

while for an infinitely small stress change $\delta\sigma$ we obtain

$$\frac{-E_t}{E_u} = \frac{1}{\dfrac{L}{w_c} - 1 + \dfrac{E_u}{Cw_c}} \tag{52}$$

If we know the dependence of tangent modulus E_t and the unloading modulus E_u on strain ε (or the dependence of average tangent modulus $\bar{E}_t$ and the averaging unloading modulus $\bar{E}_u$ on strain ε), we can determine from these equations the point of instability, as has been done by Bažant (1976). Eq. 52 thus gives the point on the stress-strain curve at which strain-localization into the crack band initiates, and Eq. 51 gives the point onthe stress-strain curve from which a complete fracture can happen.

From Eq. 52 we may observe that for support by a very soft spring, i.e., $C \to 0$, or for a very long specimen, i.e., $L/w_c \to 0$, the strain localization starts at $E_t = 0$, i.e., at the peak stress point. Therefore, in large structures, the fracture energy is given by the area in Fig. 15a limited by the unloading branch from the peak stress point. This is the maximum possible value of G_f. On the other hand, if the support provided by the surrounding structure to the fracture process zone is very stiff, $C \to \infty$, or if the volume outside the fracture process zone is very small, i.e., $L/w_c \to 1$, then according to Eq. 52 instability can happen only when $\bar{E}_t$ reaches a large value, in which case instability begins only late in the strain-softening behavior or never. It is only in such situations that the strain-softening behavior is stable and can be observed in experiments. In fact, Eq. 52 may be used to determine the maximum possible dimension of test specimen and the minimum required stiffness of the testing machine which permit the experimentalist to measure the strain-softening complete stress-strain curve.

STRAIN-SOFTENING BEHAVIOR IN GENERAL

From our preceding considerations it is clear that the simple stability analysis we demonstrated can be applied to strain-softening behavior in compression or shear. Therefore, the failures in compression and shear in geomaterials, which are typically characterized by strain-softening, should be treated either in terms of stability analysis or in terms of an equivalent fracture mechanics approach such as we demonstrated for tension. A detailed analysis cannot however be accommodated in this lecture.

In contrast to tension, the shear or compression loading of geomaterials may lead to only a partial strain-softening after which a plateau corresponding to a certain residual strength (τ_r in Fig. 15d) is reached. For such situations, it is easy to carry out a completely analogous stability analysis, from which it follows that this type of behavior must also be treated in terms of fracture mechanics or analysis of strain localization, as stated by Rice and Palmer (1973). Such a calculation shows that the fracture energy is given by an area under the strain-softening branch which is not limited at the bottom by the strain axis but by the horizontal line corresponding to the residual strength. Fig. 15d shows the area corresponding to the maximum fracture energy and the area giving the apparent fracture energy when instability starts later in the strain-softening process. (All that is necessary to do in the preceding calculation is to replace the jump from σ_p or from σ^0 to 0 by the jump from these values to σ_r.)

CONCLUSION

From the analysis presented in this lecture, we may conclude that, due to their heterogenity, the fracture of many geomaterials, including rocks as well as the artificial rock — concrete, should be treated in terms of a three-parameter fracture mechanics, involving not only the fracture energy, but also the strength and the width of the fracture process zone. The latterparameter can however be related, as a good approximation, to the size of the inhomogeneities (grain in rock or maximum aggregate size in concrete), which then leaves us with a two-parameter nonlinear fracture mechanics as a good approximation. Such a theory is in satisfactory agreement with all typical known test data. It is characteristic of our treatment that fracture is approached through the strain-softening stress-strain relations, and may be regarded as the phenomenon of strain-localization in a strain-softening continuum, in which fracture is nothing else but a strain-localization instability.

Acknowledgment

Financial support under U. S. National Foundation Grant No. CEE-8009050 is gratefully appreciated. Mary Hill is thanked for her invaluable secretarial assistance.

REFERENCES

Barenblatt, G. I. (1959). "The Formation of Equilibrium Cracks During Brittle Fracture. General Ideas and Hypothesis. Axially-Symmetric Cracks," Prikladnaya Matematika i Mekhanika, Vol. 23, No. 3, pp. 434-444.

Bažant, Z. P. (1976). "Instability, Ductility and Size Effect in Strain-Softening Concrete," J. of the Engineering Mechanics Division ASCE, Vol. 102, Apr. 1976, No. EM2, pp. 331-344, Paper 12042.

Bažant, Z. P., and Cedolin, L. (1979). "Blunt Crack Band Propagation in Finite Element Analysis," Journal of the Engineering Mechanics Division, ASCE, Vol. 105, No. EM2, Proc. Paper 14529, pp. 297-315.

Bažant, Z. P., and Cedolin, L. (1980). "Fracture Mechanics of Reinforced Concrete," Journal of the Engineering Mechanics Division, ASCE, Vol. 106, No. EM6, Proc. Paper 15917, pp. 1287-1306.

Bažant. Z. P., and Cedolin, L. (1981). "Finite Element Modeling of Crack Band Propagation in Reinforced Concrete," Center for Concrete and Geomaterials, Report No. 81-9/640f, Northwestern University, Evanston, Illinois 60201.

Bažant, Z. P., and Gambarova, P. G. (1980). "Rough Cracks in Reinforced Concrete," Journal of the Structural Division, ASCE, Vol. 106, No. ST4, Paper No. 15330, pp. 819-842.

Bažant, Z. P., and Kim, S. S. (1979). "Plastic-Fracturing Theory for Concrete," Journal of the Engineering Mechanics Division, ASCE, Vol. 105, No. EM3, Proc. Paper 14653, pp. 407-428.

Bažant, Z. P., and Oh. B. H. (1981) "Concrete Fracture via Stress-Strain Relations," Report No. 81-10/665c, Center for Concrete and Geomaterials, Northwestern University, Evanston, Illinois

Bažant, Z. P., and Panula, L. (1978). "Statistical Stability Effects in Concrete Failure," J. of the Engineering Mechanics Division, ASCE, Vol. 104, No. EM5, pp. 1195-1212, Paper 14074.

Bažant, Z. P., and Tsubaki, T. (1980). "Slip-Dilatancy Model for Cracked Reinforced Concrete," Journal of the Structural Division, ASCE, Vol. 106, No. ST9, Paper No. 15704, pp. 1947-1966.

Carpinteri, A. (1980). "Static and Energetic Fracture Parameters for Rocks and Concretes," Report, Istituto di Scienza delle Costruzioni-Ingegneria, University of Bologna, Italy.

Carpinteri, A. (1981). "Experimental Determination of Fracture Toughness Parameters K_{Ic} and J_{Ic} for Aggregate Materials", "Advances in Fracture Research," Proc., 5th International Conference on Fracture, Cannes, France, Ed. by D. François, Vol. 4 pp. 1491-1498.

Cedolin, L., and Bažant, Z. P. (1980). "Effect of Finite Element Choice in Blunt Crack Band Analysis," Computer Methods in Applied Mechanics and Engineering, Vol. 24, No. 3, pp. 305-316.

Evans, R. H., and Marathe, M. S. (1968). "Microcracking and Stress-Strain Curves for Concrete in Tension," Matériaux et Constructions, Vol. 1, No. 1, pp. 61-64.

Hillerborg, A., Modéer, M., and Petersson, P. E. (1976). "Analysis of Crack Formation and Crack Growth in Concrete by Means of Fracture Mechanics and Finite Elements," Cement and Concrete Research, Vol. 6, pp. 773-782.

Hoagland, R. G., Hahn, G. T., Rosenfield, A. R. (1973). "Influence of Microstructure on Fracture Propagation in Rock," Rock Mechanics, Vol. 5, pp. 77-106.

Kfouri, A. P., and Miller, K. J. (1974). "Stress Displacement, Line Integral and Closure Energy Determinations of Crack Tip Stress Intensity Factors," Int. Journal of Pres. Ves. and Piping, Vol. 1, No. 3, pp. 179-191.

Kfouri, A. P., and Rice, J. R. (1977). "Elastic/Plastic Separation Energy Rate for Crack Advance in Finite Growth Steps," in "Fracture 1977" (Proc. of the 4th Intern. Conf. on Fracture, held in Waterloo, Ontario), Ed. by D. M. R. Taplin, Univeristy of Waterloo Press, Vol. 1, pp. 43-59.

Knauss, W. G. (1974). "On the Steady Propagation of a Crack in a Viscoelastic Sheet; Experiments and Analysis," Reprinted from The Deformation in Fracture of High Polymers, Ed. by H. H. Kausch, Publ. Plenum Press, pp. 501-541.

Knott, J. F. (1973). "Fundamentals of Fracture Mechanics," Butterworths, London, England.

Kupfer, H. B., and Gerstle, K. H. (1973). "Behavior of Concrete under Biaxial Stress," Journal of the Engineering Mechanics Division, ASCE, Vol. 99, No. EM4, Proc. Paper 9917, pp. 853-866.

Liu, T. C. Y., Nilson, A. H., and Slate, F. O. (1972). "Biaxial Stress-Strain Relations for Concrete," Journal of the Structural Division, ASCE, Vol. 98, No. ST5, Proc. Paper 8905, pp. 1025-1034.

Løland, K. E. (1980). "Continuous Damage Model for Load-Response Estimation of Concrete," Cement and Concrete Research, Vol. 10, pp. 395-402.

Lorrain, M. (1981). "On the Application of the Damage Theory to Fracture Mechanics of Concrete," A State-of-the-Art Report, Civil Engineering Department, I.N.S.A., 31077 Toulouse, Cedex, France.

Mazars, J. (1981). "Mechanical Damage and Fracture of Concrete Structures," 5th International Conference on Fracture, Edited by D. François, Cannes, France, Vol. 4, pp. 1499-1506.

Oh, B. H.(1982). Private Communication on Doctoral Research in Preparation at Center for Concrete and Geomaterials, Northwestern University, Evanston, Illinois.

Palmer, A. C., and Rice, J. R. (1973). "The Growth of Slip Surfaces in the Progressive Failure of Overconsolidated Clay," Proc. of the Royal Society, London, Series A, Vol. 332, pp. 527-548.

Rice, J. R. (1976). "The Localization of Plastic Deformation," Preprints, 14th Congress of the International Union for Theoretical and Applied Mechanics, Delft, Netherlands, pp. 207-220.

Petersson, P. E. (1980). "Fracture Energy of Concrete: Method of Determination," Cement and Concrete Research, Vol. 10, pp. 78-89, and "Fracture Energy of Concrete: Practical Performance and Experimental Results," Cement and Concrete Research, Vol. 10, pp. 91-101.

Schmidt, R. A. (1976). "Fracture-Toughness Testing of Limestone," Experimental Mechanics, Vol. 16, No. 5, pp. 161-167.

Schmidt, R. A. (1977). "Fracture Mechanics of Oil Shale - Unconfined Fracture Toughness, Stress Corrosion Cracking, and Tension Test Results," Proc. 18th U. S. Symp, Rock Mechs., Paper 2A2, Colo. School of Mines, Golden, Co.,

Schmidt, R. A., and Lutz, T. J. (1979). "K_{ic} and J_{ic} of Westerly Granite — Effect of Thickness and In-Plane Dimensions," ASTM STP 678, Ed. by S. W. Freiman, American Society for Testing and Materials, Philadelphia, Pa., pp. 166-182.

Suidan, M., and Schnobrich, W. C. (1973). "Finite Element Analysis of Reinforced Concrete," Journal of the Structural Division, ASCE, Vol. 99, No. ST10, Oct. 1973, pp. 2109-2122.

Wnuk, M. P. (1974). "Quasi-Static Extension of a Tensile Crack Contained in Viscoelastic Plastic Solid," Journal of Applied Mechanics, ASME, Vol. 41, No. 1, pp. 234-248.